Air infiltration and related building energy consumption
A case study of office buildings in Changsha, China

Hu, Jie; Liu, Zhengxuan; Ma, Guochuan; Zhang, Guoqiang; Ai, Zhengtao

DOI
10.1016/j.jobe.2023.106859

Publication date
2023

Document Version
Final published version

Published in
Journal of Building Engineering

Citation (APA)
Hu, J., Liu, Z., Ma, G., Zhang, G., & Ai, Z. (2023). Air infiltration and related building energy consumption: A case study of office buildings in Changsha, China. *Journal of Building Engineering*, *74*, Article 106859. https://doi.org/10.1016/j.jobe.2023.106859

Journal of Building Engineering 74 (2023) 106859

Contents lists available at ScienceDirect

Journal of Building Engineering

journal homepage: www.elsevier.com/locate/jobe

Air infiltration and related building energy consumption: A case study of office buildings in Changsha, China

Jie Hu [a,b], Zhengxuan Liu [a,b,c], Guochuan Ma [d], Guoqiang Zhang [a,b,*], Zhengtao Ai [a,b,**]

[a] Department of Building Environment and Energy, College of Civil Engineering, Hunan University, Changsha, Hunan, China
[b] National Center for International Research Collaboration in Building Safety and Environment, Hunan University, Changsha, Hunan, China
[c] Faculty of Architecture and the Built Environment, Delft University of Technology, Julianalaan 134, 2628 BL, Delft, the Netherlands
[d] China Southwest Architectural Design and Research Institute, Chengdu, Sichuan, China

ARTICLE INFO

Keywords:
Airtightness
Tracer gas method
Air-conditioning system
EnergyPlus
Infiltration-related energy consumption

ABSTRACT

Past studies reveal that air infiltration through the building envelope and its impact on the indoor environment and energy consumption are significantly influenced by climate characteristics. However, little relevant information is available for buildings in southern China, where the building design traditionally follows a philosophy of being open and shaded. The present study employs both experimental measurements and numerical simulations to investigate the airtightness of buildings in Hot Summer and Cold Winter (HSCW) climate region of southern China and the associated energy consumption. The measurements and simulations are based on a typical office building in Changsha. Measurement results show that the air infiltration rate of six tested spaces at the natural pressure difference ranges from 0.10 to 0.30 h^{-1} with an average of 0.17 h^{-1} in summer, and from 0.09 to 0.32 h^{-1} with an average of 0.16 h^{-1} in winter. The operation of the air-conditioning system affects largely air infiltration, and each unit change in setpoint air temperature can result in an average of one-third or more change in air infiltration rate. Simulation results show that a decrease in air infiltration rate from 0.17 h^{-1} to 0.01 h^{-1} reduces the infiltration-related cooling energy consumption from 14.29 to 0.75 kWh/m^2·year and heating energy consumption from 8.20 to 0.39 kWh/m^2·year. The same change in the setpoint air temperature of air-conditioning system in summer and winter results in different infiltration-related energy consumption. The findings would contribute to an improved energy simulation and assessment of buildings in southern China.

1. Introduction

Past studies have shown that air infiltration has various effects on many aspects of buildings, such as indoor acoustic environment [1], indoor air quality (IAQ) [2], thermal comfort [3,4], building envelope thermal performance [5,6], and building energy consumption. A study [2] reported a direct correlation between airtightness and indoor air quality, which showed that increased airtightness reduced the infiltration of outdoor pollutants. Moreover, improved airtightness would reduce the penetration of outdoor water vapor and lower the transmission of outdoor noise.

* Corresponding author. Department of Building Environment and Energy, College of Civil Engineering, Hunan University, Changsha, Hunan, China.
** Corresponding author. Department of Building Environment and Energy, College of Civil Engineering, Hunan University, Changsha, Hunan, China.
E-mail addresses: gqzhang@188.com (G. Zhang), zhengtaoai@hnu.edu.cn (Z. Ai).

https://doi.org/10.1016/j.jobe.2023.106859
Received 23 February 2023; Received in revised form 23 April 2023; Accepted 15 May 2023
Available online 16 May 2023

International agencies and countries have put forward requirements for the energy performance of buildings in their current national regulations or design standards, such as the International Energy Conservation Code (IECC), the French Energy Performance Code RT2012, and the American ASHRAE 62.2 and 90.1. However, they have formulated distinct requirements for the airtightness of ordinary buildings. As shown in Table 1, Nordic countries such as Finland and Denmark have stricter airtightness requirements than Southern European countries. The current airtightness requirement for near-zero energy buildings (nZEB) in Central, Northern Europe, and China is that the N_{50} is not higher than 0.6 h^{-1} [7].

To reveal whether the building airtightness is up to standard, it is necessary to perform extensive airtightness measurements on existing buildings. The widely applied test standards are ISO 9972: 2015 [10] and ASTM E741-11 [11]. At the end of 2020, China implemented the standard T/CECS 704–2020 [12], which is the testing and evaluation standard for building airtightness in line with Chinese conditions. This standard describes in detail the airtightness technical methods and proposes the specific classification of building airtightness. According to the above standards, plenty of airtightness measurements have been carried out around the world, especially in the United States and Europe, and some typical results are summarized in Table 2. However, there is a lack of tests on airtightness of buildings in southern China.

The air infiltration through the building is affected by many factors. To establish a fast and accurate airtightness prediction model and to better evaluate the building airtightness, it is necessary to delve into these influencing factors, such as construction method [8], air-conditioning system [15], building height/number of floors [13,27], building area, building typology [15,28], year of construction [16,29], climate region [6], decoration/renovation [30,31], and process quality and maintenance [13,20]. In addition, Salehi [20] found that architectural attributes such as building geometry and the quality of interventions had a greater impact on infiltration and ventilation rate than building typology. Feijó-Muñoz et al. [6] reported that building location and window material were also statistically significant parameters that had a great effect on air infiltration. It is necessary to analyze and compare building airtightness by considering various influencing factors.

Numerous studies have been conducted to assess the impact of air infiltration on energy consumption. It was found that the heat loss caused by infiltration accounts for 25–50% of the total building load [1]. Tommerup et al. [32] found a 10% increase in energy consumption for every degree of increase or decrease in indoor temperature caused by the infiltration of single-family houses in Denmark. To further clarify the effect of air infiltration on building energy consumption, another study [33] estimated that improving the airtightness of the building envelope could reduce the heating demand by 10 kWh/(m^2·a) in areas with a heating degree day of 2500 (°C·d). Wang et al. [34] used the airtightness measurement results of existing apartments to simulate office buildings in different climatic regions based on Characteristic Temperature Method (CTM) and concluded that the annual heating/cooling energy consumption of buildings would increase after improving the building airtightness, while the heating energy consumption increases more. Jokisalo et al. [35] used the IDA-ICE tool to simulate the infiltration of Finnish detached houses, and the results showed that for every 1.0 h^{-1} change in air infiltration rate at 50 Pa pressure difference, the heating energy consumption caused by air infiltration was changed by 4–12%, while the total heating energy consumption changed by 2–7%. In general, past studies on the impact of air infiltration on energy consumption were mostly carried out using various simulation methods. However, some studies, such as Šadauskienė et al. [36], indicated that the calculation of building energy consumption can be reliable only with the verification of the airtightness. Therefore, it is important to combine the airtightness measurement with energy consumption simulation.

However, there are still some important but under-attended research gaps in this topic, mainly on the following aspects: (1) Most of the past studies regarding airtightness focus on residential buildings, while office buildings have been paid less attention; (2) Most of the past studies regarding energy consumption simulations are based on air infiltration through buildings under natural condition, but the operation of air-conditioning systems in buildings leads to the change in air infiltration, which inevitably modifies the infiltration related energy consumption; (3) The air infiltration through the building varies with climate region. The design airtightness of buildings is relatively high in Nordic countries and Northern China, where the insulation of building envelope is important. However, airtightness is not emphasized during the early design of buildings in the HSCW climate region of China (i.e., a typical region in Southern China), and thus its influence on building energy consumption is still not clear.

The contributions of the present study would be to (1) reveal the air infiltration level of office buildings in Changsha (i.e., a typical city in the HSCW climate region) with and without air-conditioning system running through on-site measurements, (2) determine quantitatively the influence of the operation of the air-conditioning system on air infiltration, and (3) evaluate the energy consumption of buildings based on the measured airtightness data.

Table 1
Airtightness requirements of ordinary buildings in some countries [8,9].

Countries	N_{50}/h^{-1}
Finland	$N_{50} \leq 1.0$
Denmark	$N_{50} \leq 2.8$
Sweden	$1.0 \leq N_{50} \leq 3.0$
Norway	$N_{50} \leq 3.0$
Switzerland	$N_{50} \leq 3.6$
Germany	$1.8 \leq N_{50} \leq 3.6$
The Netherlands	$N_{50} \leq 6.0$
US	$N_{50} \leq 5.4$

Table 2
Typical airtightness measurement results of ordinary buildings in various countries.

Location	Year of buildings	Type of buildings	Number of buildings	Average value	
				Q_{50}/m^3/(m^2·h)	N_{50}/h^{-1}
Estonia [13]	2003–2005	Single-family house	32	4.20	4.90
Greece [14]	2005	Single-family house	20	–	7.00
UK [8]	2006	Single-family house	287	5.97	–
Ireland [15]	1944–2008	Single-family house	28	9.10	–
US [16]	1932–1999	Single-family house	134000	–	2.90–40.50
Finland [17]	2002–2005	Single-family house	56	–	1.60
Italy [18]	1810–2010	Single-family house	20	–	3.20–8.50
The Netherlands [19]	2017	Single-family house	44	–	2.65
Portugal [20]	2017	Single-family house	4	–	5.48–9.63
France [21]	1871–2004	Multi-family house	567	–	0.49 (Natural pressure)
Spain [6]	1890–2015	Multi-family house	171	6.56	–
Canada [22]	2007–2019	Multi-family house	12	1.76	–
South Korea [23]	2005–2006	Multi-family house	45	–	0.26 (Natural pressure)
Beijing, China [24]	1990–2010	Multi-family house	34	–	0.85–10.03
Tangshan, China [25]	1990	Multi-family house	1	–	16.70
Dalian, China [3]	2013–2015	Multi-family house	4	–	1.77
Qingdao, China [26]	2016	Public building	1	–	0.30

2. Methodology

The framework diagram of the present study is shown in Fig. 1. The basic idea is firstly to measure the air infiltration rate of the office building with and without air-conditioning system running and to analyze the influencing factors, secondly to build complete metamodels in EnergyPlus and to identify the uncertainty parameters, thirdly to establish the model of an appropriate air-conditioning system according to the climate characteristics and to define the system operational schedule, and finally to input air infiltration rate obtained from measurements and thermal disturbance parameters into EnergyPlus to perform simulations.

2.1. Experimental method

2.1.1. Typical building for measurement

The selected building for measurement is located in Changsha, one of the major cities in the HSCW climate region in China, with an average altitude of 68 m. The yearly average air temperature in Changsha is 17.5 °C, while the average temperature in the coldest and warmest months is 4–8 °C and 27–30 °C. The yearly average relative humidity is about 75% and the average wind speed is 2.89 m/s [37]. The selected six-story office building was built in 2010 and has a total area of 909.66 m^2. Table 3 shows the envelope characteristics of this building, which are consistent with the relevant standards and are thus typical in this climate region. Fig. 2 shows the layout of the fourth floor, where the spaces marked in green are the office spaces selected for measurement.

2.1.2. Measurement method

The feasibility of using tracer gas to measure air infiltration rate has been verified by numerous experimental studies [14,22,36,38]. According to ASTM E741-11 [11], the most widely used tracer gas method is the concentration decay method [39]. Another widely used method, namely the fan pressurization method, could reduce or rise the atmospheric pressure inside the building so that the cracks and openings of the building can be enlarged to some extent [40]. In addition, the accuracy of investigating the airtightness of the building with the tracer gas method has been well proved [41], which was therefore selected in the present study.

In the present study, all measurements were made according to ASTM E741-11 and T/CECS 704–2020 [12]. CO_2 [42] was chosen as the tracer gas for tests, where each space was tested separately. Several repeated measurements were carried out for each specific condition. The regressive total volume for all tested spaces meets the volume requirements for measurements based on the maximum volume space of the building. The measurements were performed under the following conditions.

(1) The outdoor wind speed did not exceed 3 m/s; and
(2) The exterior doors and windows of each tested space were closed; the doors and windows that communicate with the untested spaces were closed; the sockets were sealed and the pipe holes were filled.

Table 4 lists the parameters of measuring instruments used in the present study. TESTO-480 with the highest accuracy was used to measure the evolution of CO_2 concentration that was eventually used to calculate the air infiltration rate. Several sets of Telaire T7001 were used to determine whether CO_2 was homogeneously mixed, which were equipped with a HOBO data recorder. HT-2000 was used to measure outdoor CO_2 concentration. These CO_2 instruments were cross-calibrated before measurements.

2.1.3. Experimental process

Because of the completely different climate conditions in summer and winter in Changsha, the measurements were conducted both in summer and winter in the year 2021. Fig. 3(a) shows the global view of the tested spaces, while the furniture was retained because relevant studies have shown that the presence of furniture has a certain impact on ventilation efficiency [43]. During the measurements, the indoor and outdoor temperatures and the outdoor wind speed were recorded simultaneously. As shown in Fig. 3(a), the

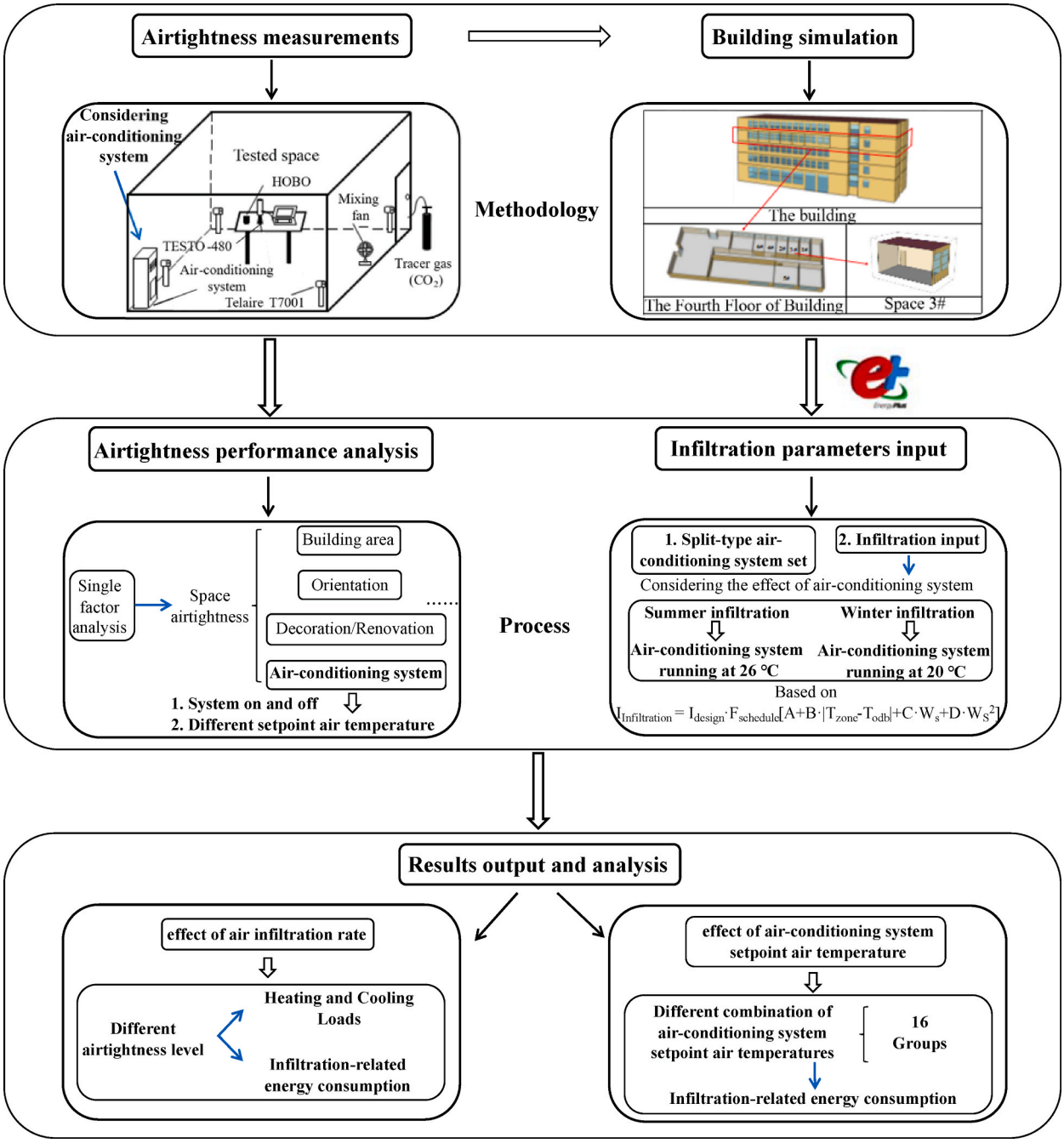

Fig. 1. The framework diagram of the present study based on airtightness measurements and infiltration-related energy consumption simulation.

Table 3
The envelope characteristics of the tested building.

Building Envelope	Material	Thickness/mm	U-value/w/(m^2·k)
Exterior wall	Polystyrene board, Reinforced concrete, Cement mortar	360	0.618
Interior wall	Concrete block, Cement mortar	240	0.429
Exterior window	Hot aluminum alloy, Insulating glass	3 + 13A + 3	2.720
Interior ceiling	Reinforced concrete, Cement mortar, Waterproof roll	150	0.556

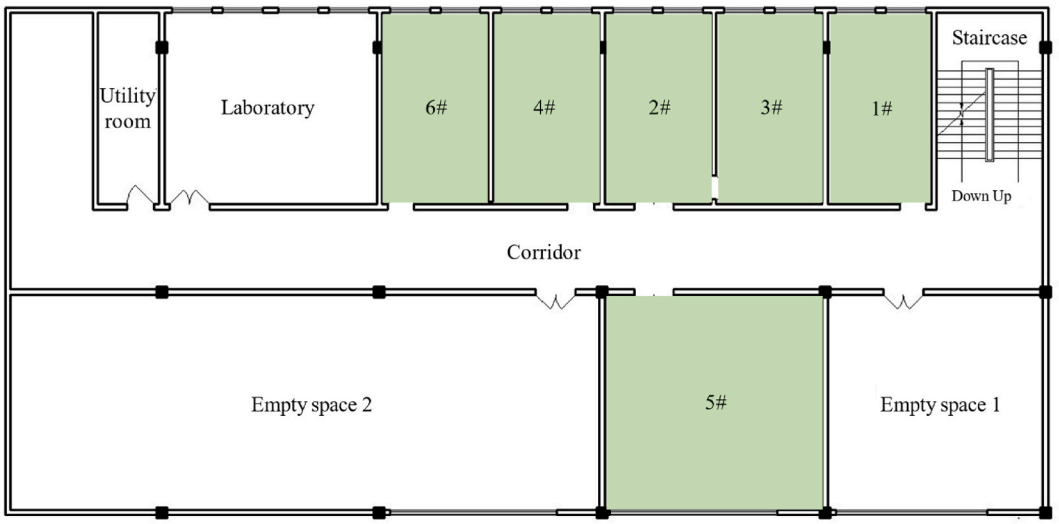

Fig. 2. The layout of the typical floor and the typical office spaces (marked in green) selected for measurement. (For interpretation of the references to colour in this figure legend, the reader is referred to the Web version of this article.)

Table 4
The detailed information of the measuring instruments.

Measuring Instrument	Measurement Parameters	Measuring Range	Accuracy	Amount
CO_2 Gas Flowmeter	CO_2 flow rate	0–1 L/min	–	2
Telaire T7001	CO_2 concentration	0–10000 ppm	±5%	4
TESTO-480		0–10000 ppm	±3%	1
HT-2000		0–9999 ppm	±5%	1
TESTO-440	Outdoor wind speed	0–20 m/s	± (0.03 m/s+4% measured value)	1
HOBO UX100-003	Temperature	−20–70 °C	±0.21 °C	2
	Relative humidity	15%–95%	±3.5%	
Laser Distance Meter	Size of the envelope	0.2–60 m	± (2 mm + 5 × 10^{-5}D)	1

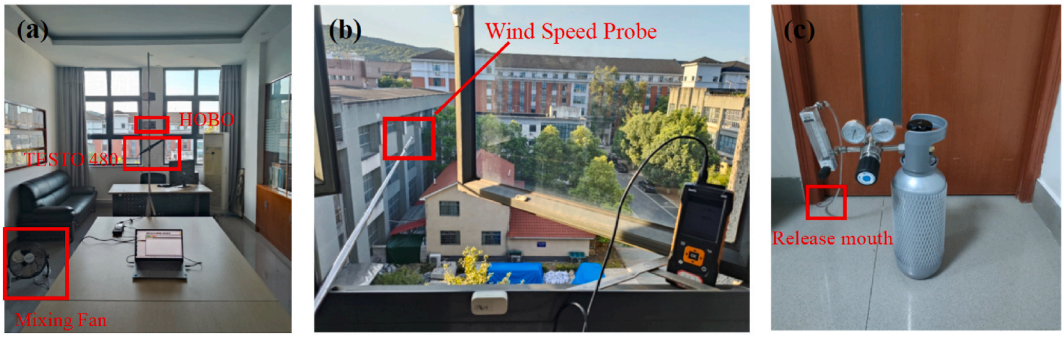

Fig. 3. Layout of the tested spaces: (a) Global view, (b) Outdoor wind speed measurement location, and (c) CO_2 release location.

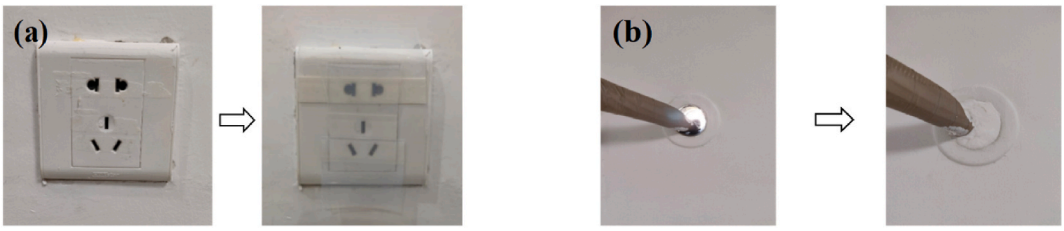

Fig. 4. Sealing measures in the tested spaces: (a) Socket sealing, and (b) Pipe hole filling.

HOBO sensor for the indoor air temperature measurement point was located in the center of the space. As the outdoor wind speed has a significant effect on the building airtightness [44], the outdoor wind speed was measured with the measurement point set at 1.0 m from the exterior wall of the adjacent space (as shown in Fig. 3(b)). The release of tracer gas CO_2 was accurately controlled by pressure reducing valve and gas flowmeter (as shown in Fig. 3(c)).

The socket holes were treated with waterproof sealing tape, as shown in Fig. 4(a), and the gap between the hose of the air conditioner for refrigerant and the wall was treated with sealant, as shown in Fig. 4(b).

A split type of air conditioner was installed in each tested space, which does not have an air duct to connect the indoor to the outdoor or other spaces. The cooling and heating capacity of the air conditioner is 7200 W and 9600 W, respectively. Four setpoints of indoor air temperature at 22, 24, 26, and 28 °C were considered in summer and four setpoints at 18, 20, 22, and 24 °C in winter. The air conditioner was controlled remotely. The air was supplied from the upper part of the room, which can enhance the uniform mixing of CO_2 indoors and prevent the air supply from directly affecting the measuring instruments. To ensure the stability of the indoor air temperature during the measurements, the air conditioner was always in operation from before the release of CO_2 until the end of the measurements.

Based on the measured data, the $\overline{N}$ of the tested space was calculated from Eq. (1) [11].

$$\overline{N} = [lnC(t_2) - lnC(t_1)] / (t_2 - t_1) \tag{1}$$

where $\overline{N}$ is the mean air infiltration rate, h^{-1}; C is the indoor CO_2 concentration at a certain time, ppm; and t_1, t_2 are the measurement time, h.

To further characterize the air infiltration through the building envelope, the equation of air permeability [11] was written as:

$$q = \overline{N} \cdot V \tag{2}$$

where q is the air permeability under a certain indoor and outdoor pressure difference, m^3/h; and V is the volume of the tested space, m^3.

Based on the volume of each tested space, the weighted mean air infiltration rate can be calculated and taken to indicate the airtightness of the whole floor of the building. According to the standard [12], Eq. (3) was derived in this study.

$$\overline{N}_s = \sum_{i=1}^{n} \overline{N}_{i\#} \cdot \frac{V_{i\#}}{V_{whole}} (i \le 6, n = 6) \tag{3}$$

where $\overline{N}_s$ is the average air infiltration rate of the whole standard floor of the building, h^{-1}; $\overline{N}_{i\#}$ is the air infiltration rate of each tested space, h^{-1}; $V_{i\#}$ is the volume of each space, m^3; and V_{whole} is the total volume of all spaces on the standard floor, m^3.

According to Table 2, the most widely used indicator of airtightness is N_{50}. Sherman [45] obtained the conversion model for the prediction of air permeability under 50 Pa pressure difference and natural pressure difference as in Eq. (4) concerning the classic K–P model.

$$ACH_{50} = ACH \cdot n \tag{4}$$

where n is the correlation coefficient, which is related to the local climate, stack effect, wind force, and infiltration type. The standard DB11/T 555–2015 [46] points out that the n of China is taken as 17.

In this study, the air leakage paths (ALPs) of the building were also tested. Since specific information about the interior of the building, such as the length and path of cracks within the walls, was not available, smoke pens were used to detect and confirm the typical air leakage paths of the building envelope. As shown in Fig. 5, air leakage was roughly determined by observing the smoke flow in the tested area, especially for individual components such as doors and windows. Note that high-precision instruments such as infrared thermal imager are required to detect a specific leakage distribution [47], but this is not the focus of the present study.

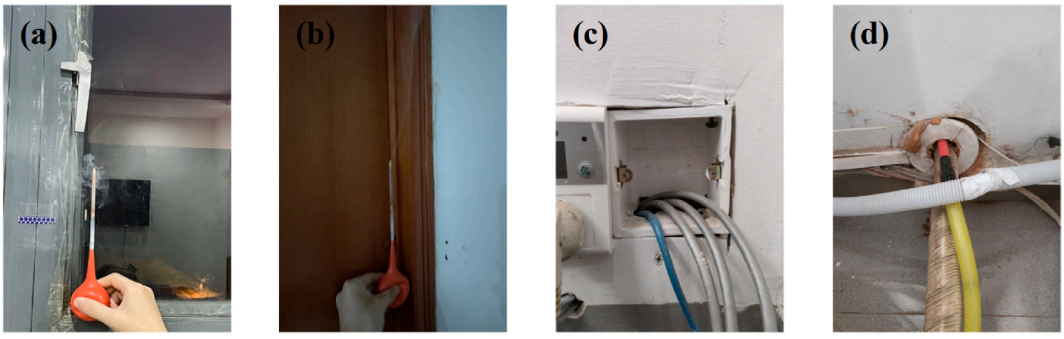

Fig. 5. Approximate detection of air leakage paths: Smoke pen test: (a) Exterior window and (b) Interior door; Direct observation: (c) Socket base and (d) Through-wall pipeline.

2.2. Simulation method

2.2.1. Building model

In the present study, SketchUp was used to build the geometry, and the commercial platform EnergyPlus was used to simulate building energy consumption. The EnergyPlus was widely recognized and used in past studies [28,48–52]. Hu et al. [52] have previously validated the EnergyPlus model based on the same office building model as used in the present study, justifying our simulations.

As the parameters, such as building and indoor geometries, ventilation condition, and indoor occupancy rate, determine the simulation accuracy and reliability of building energy consumption [53], they were accurately defined based on the measured building and results.

2.2.2. Simulation process

The air-conditioning system considered in the present study is the Packaged Terminal Heat Pump that is only running in summer and winter. It is assumed that the design air temperature of cooling and heating seasons in the HSCW climate region is 26 °C and 20 °C, respectively. Parameters such as heat dissipation of humans, equipment, and lighting in the tested space were set in conformity with the standard GB 55015-2021 [54], as shown in Table 5. The activity level of people was treated as sedentary, and the schedules of the occupancy, equipment usage, and lighting were set according to the real-life condition, which was presented in Fig. 6. The electricity was the only source of energy consumption for cooling, heating, and fans.

The period considered for simulations was throughout the year 2021, namely, from January 01 to December 31, and the meteorological data during that period obtained from the Changsha Climate Meteorological Data Source was used. The time step of simulations was set to be 4 times per hour, which would give a sufficiently dynamic response.

Two infiltration modes were considered and compared, i.e., Mode 1 – infiltration only in summer and winter, with natural ventilation during shoulder season (air change rate under natural ventilation is set to 5.0 h^{-1}), and Mode 2 – infiltration throughout the year. The building cooling/heating loads simulation was performed first to identify the more suitable one between Mode 1 and Mode 2 by analyzing the relationship between load and airtightness, and then the energy consumption simulations were conducted based on the identified mode.

In the subsequent energy consumption simulations, the air infiltration rate measured at 26 °C in summer and 20 °C in winter were defined as the mean air infiltration rate in summer and winter, respectively.

The infiltration models constructed in the present study were based on the NIST (National Institute of Standards and Technology) infiltration correlations [49], which were developed using the CONTAM models of the DOE prototype buildings and weather files. Infiltration between zones needed to be set by the Zone Infiltration module in EnergyPlus. If the energy consumption is predicted according to the mean air infiltration rate of the building, results would be quite different from the real-life data. To tackle this problem, the total energy consumption was obtained by simulating separately each tested space and adding them up. The obtained data were input into the Design Flow Rate in the module of Zone Infiltration Schedule, which was adopted as the algorithm for air infiltration rate. Therefore, in the corresponding empirical Eq. (5) for the infiltration simulation based on the NIST infiltration correlations, the constant coefficient A was set to 1.0 and the other coefficients B, C and D were set to 0 (because the effect of wind speed is not considered).

$$I = I_{design} \cdot F_{schedule}\left[A + B \cdot |T_{zone} - T_{odb}| + C \cdot W_s + D \cdot W_s^2\right] \tag{5}$$

where I is the calculated infiltration rate of the building, h^{-1}; I_{design} is the designed infiltration rate of the building, h^{-1}; T_{zone} and T_{odb} is the indoor and outdoor pressure, Pa; and W_s is the outdoor wind speed, m/s. In this model, when the air-conditioning system is turned on, $F_{schedule}$ is set to 1.0; when the system is off, it is 0.

The influence of airtightness level on building energy consumption was examined by considering different airtightness levels. As shown in Table 6, the entered air infiltration rate for each airtightness level was the middle value of the corresponding interval. The construction of the case will not be realistic when the air infiltration rate is lower than 0.01 h^{-1} (an actual building is not completely airtight), so it is assumed that 0.01 h^{-1} is the lowest value that can be achieved.

Table 5
The geometry and indoor heating sources of the tested spaces.

	Area/ m^2	Volume/ m^3	Envelope area/ m^2	Window glass area/ m^2	Conditioned (Y/ N)	Number of persons	Light/W/ m^2	Equipment/W/ m^2
1#	28.08	89.86	82.14	6.30	Yes	1	9	5
2#	28.80	92.16	82.88	6.30	Yes	1	9	5
3#	28.80	92.16	82.88	6.30	Yes	1	9	5
4#	28.80	92.16	82.88	6.30	Yes	7	9	15
5#	64.80	207.36	119.14	13.23	Yes	7	9	15
6#	28.80	92.16	82.88	6.30	Yes	14	9	15
Total	208.08	665.86	532.8	44.73	–	–	–	–

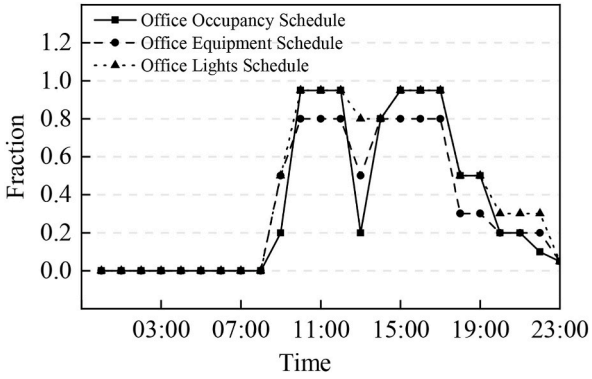

Fig. 6. Schedule of occupancy, equipment, and lights in the tested office building.

Table 6
The standard and entered air infiltration rate corresponding to different airtightness levels according to T/CECS 704–2020.

Airtightness level	Level 1	Level 2	Level 3	Level 4	Level 5	Level 6	Level 7	Level 8
Standard value/ h^{-1}	$N > 0.3$	$0.2 < N \leq 0.3$	$0.13 < N \leq 0.2$	$0.08 < N \leq 0.13$	$0.05 < N \leq 0.08$	$0.03 < N \leq 0.05$	$0.015 < N \leq 0.03$	$N \leq 0.015$
Entered value/h^{-1}	Actual value	0.25	0.165	0.10	0.065	0.04	0.02	0.01

3. Results and discussion

3.1. Airtightness measurements

3.1.1. Measurements without air-conditioning system running

The CO_2 variation before and during the whole measurement is shown in Fig. 7. This includes a 15-min release phase and a 5-min waiting phase for homogeneous mixing. The completely mixing status was assumed to be established after the waiting phase. Since space 5# has the largest volume, it takes longer to release and mix CO_2 in this space.

The average values of $\overline{N}$ and $\overline{N}_{50}$ for repeated measurements of each space under the natural condition in summer and winter are listed in Table 7. Table 7 also shows the average indoor and outdoor air temperature for each space and outdoor wind speed during the relevant measurement period.

The results show that the airtightness of the six spaces is considerably different, but the $\overline{N}$ values of all these spaces are less than 0.5 h^{-1}. The mean $\overline{N}$ value of the six spaces under the condition without the air-conditioning system is 0.17 h^{-1}. The airtightness performance is evaluated simultaneously by both the indicators of $\overline{N}$ and q is more accurate because different space areas would result in different q, though the $\overline{N}$ values are the same.

The airtightness of the tested building is compared with the requirements stipulated by different countries. The $\overline{N}_s$ of standard floor obtained by Eq. (3) is 0.17 h^{-1} in summer and 0.16 h^{-1} in winter. According to Table 1, the airtightness of the measured building meets the airtightness requirements of most European and American countries except for Finland. The whole airtightness level can be classified as Level 3 according to the standard T/CECS 704–2020. The requirements for building airtightness in different climate

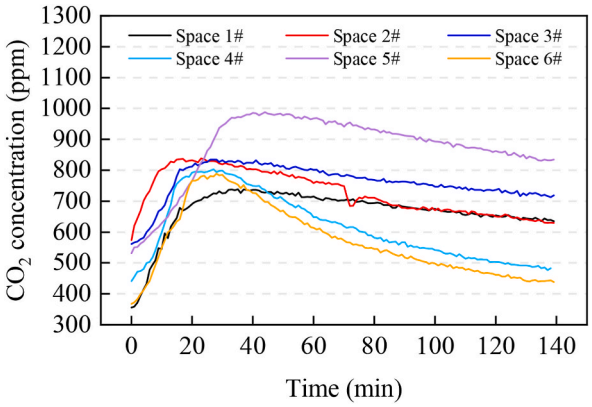

Fig. 7. The evolution of CO_2 concentration during the mixing and decay phases in each space.

Table 7
The value of airtightness and the environmental parameters during the measurements under different conditions: "N" in the column of "Measurement Conditions" denotes the measurement is performed under natural condition, without air-conditioning system running; and "×× °C" denotes the measurement is performed at specific air-conditioning setpoint air temperature.

Measurement Conditions	$\overline{N}$/h^{-1}	$\overline{N}_{50}$/h^{-1}	q/m^3/h	Air temperature/°C		V_{wind}/m/s
				Indoor	Outdoor	
1# winter case- N	0.09	1.53	8.09	15.0	11.4	0.10–1.16
1# winter case - 20 °C	0.13	2.21	11.68	19.8	7.6	0.01–1.97
1# summer case - N	0.11	1.87	9.88	31.7	38.1	0.08–2.00
1# summer case - 26 °C	0.14	2.38	12.58	26.4	37.6	0.03–1.22
2# winter case - N	0.14	2.38	12.90	17.4	13.3	0.05–1.10
2# winter case - 18 °C	0.18	3.06	16.59	17.8	6.2	0.05–1.64
2# winter case - 20 °C	0.21	3.57	19.35	19.4	12.9	0.05–1.10
2# winter case - 22 °C	0.26	4.42	23.96	21.2	14.0	0.02–1.33
2# winter case - 24 °C	0.27	4.59	24.88	23.3	11.6	0.02–0.91
2# summer case - N	0.15	2.55	13.82	31.2	35.3	0.03–1.54
2# summer case - 28 °C	0.23	3.91	21.20	28.2	36.0	0.10–2.45
2# summer case - 26 °C	0.26	4.42	23.96	26.5	34.6	0.01–0.82
2# summer case - 24 °C	0.29	4.93	26.73	23.8	34.6	0.02–1.18
2# summer case - 22 °C	0.32	5.44	29.49	21.1	34.3	0.04–1.38
3# winter case - N	0.09	1.53	8.29	11.0	4.5	0.02–0.90
3# winter case - 18 °C	0.13	2.21	11.98	17.6	6.2	0.02–2.85
3# winter case - 20 °C	0.15	2.55	13.82	19.9	4.6	0.01–0.91
3# winter case - 22 °C	0.16	2.72	14.75	21.5	3.7	0.04–1.88
3# winter case - 24 °C	0.19	3.23	17.51	23.7	5.9	0.04–1.80
3# summer case - N	0.10	1.70	9.22	29.2	35.4	0.01–1.45
3# summer case - 28 °C	0.13	2.21	11.98	28.6	35.9	0.11–2.64
3# summer case - 26 °C	0.15	2.55	13.82	26.7	29.7	0.01–0.53
3# summer case - 24 °C	0.18	3.06	16.59	24.2	26.8	0.03–1.46
3# summer case - 22 °C	0.23	3.91	21.20	22.4	34.9	0.02–0.85
4# winter case - N	0.28	4.76	25.80	15.5	11.2	0.03–1.03
4# winter case - 20 °C	0.36	6.12	33.18	20.4	16.1	0.05–1.30
4# summer case - N	0.25	4.25	23.04	31.7	38.4	0.06–1.79
4# summer case - 26 °C	0.33	5.61	30.41	26.1	36.7	0.05–1.53
5# winter case - N	0.10	1.70	20.74	19.2	9.4	0.02–1.86
5# winter case - 20 °C	0.13	2.21	26.96	19.1	8.2	0.03–0.65
5# summer case - N	0.13	2.21	26.96	31.9	35.3	0.05–1.62
5# summer case - 26 °C	0.21	3.57	43.55	26.7	35.6	0.02–1.18
6# winter case - N	0.32	5.44	29.49	13.3	3.9	0.02–1.97
6# winter case - 20 °C	0.34	5.78	31.33	19.4	6.7	0.07–1.85
6# winter case - N	0.30	5.10	27.65	30.1	35.4	0.01–1.21
6# summer case - 26 °C	0.39	6.63	35.94	26.8	38.5	0.10–0.84

regions are different, but such detailed limit values for office buildings of the HSCW climate region in China are still not available.

3.1.2. Measurements with air-conditioning system running

The operation of the air conditioning system changes the indoor air pressure fluctuation and thermally buoyancy pressure, which eventually affect the air infiltration through the envelope. In this study, the effect of the air-conditioning system on the air infiltration rate was revealed through a comparative analysis of the data obtained from the tests. Table 7 shows the measurement results with the air-conditioning system running. The mean air infiltration rate of the six spaces under the condition with the air-conditioning system

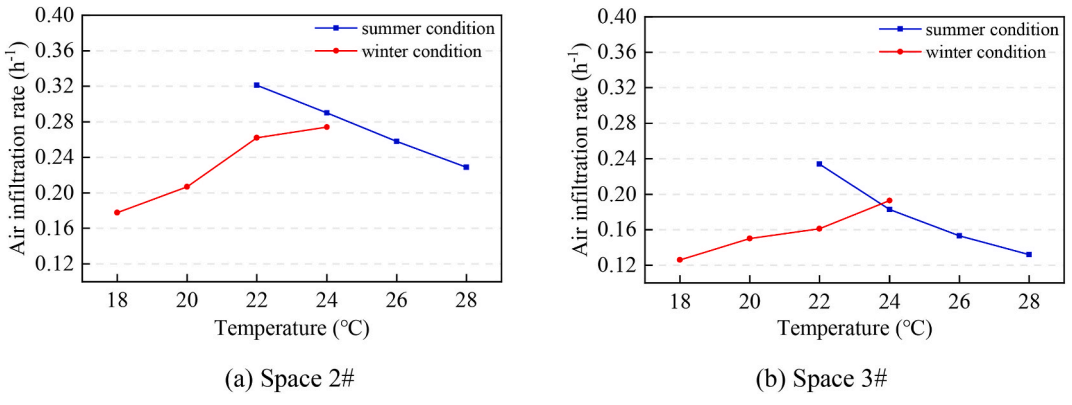

Fig. 8. The air infiltration rate of spaces 2# and 3# at different air-conditioning system setpoint air temperatures in summer and winter.

running at the setpoint air temperature of 26 °C is 0.25 h^{-1} in summer, while it is 0.22 h^{-1} at the setpoint air temperature of 20 °C in winter. Together with the analysis described in Section 3.1.1, it is clearly shown that the running of the air-conditioning system largely accelerates air infiltration through a space. In this way, air infiltration through buildings should be analyzed both with and without the air-conditioning system running.

The effect of setpoint air temperature on air infiltration was further evaluated based on the measurements in spaces 2# and 3# with the air-conditioning system running. As shown in Fig. 8, air infiltration through the space is influenced by the rise or fall of indoor air temperature, and the influence in the two spaces has generally the same trend. All other spaces in this building and in other buildings are likely to follow this trend.

For space 2#, the $\overline{N}$ value with the air-conditioning system running is 1.53–2.14 and 1.27–1.96 times higher than that without the air-conditioning system running in summer and winter, respectively, while for space 3# the value is 1.32–2.34 and 1.40–2.14. The $\overline{N}$ in space 2# is increased by 28.7% when the setpoint air temperature is dropped from 28 to 22 °C, while it is 43.6% for space 3#. The $\overline{N}$ is increased by 35.0% when the setpoint temperature is risen from 18 to 24 °C in space 2#, while it is 34.7% for space 3#.

In general, the air infiltration rate increases when the setpoint air temperature drops in summer and rises in winter. From the analysis made in the previous paragraph, the degree of change in air infiltration rate varies widely from space to space when the setpoint air temperature is changed from 28 to 22 °C, perhaps due to the insufficient number of samples. The results can also show that each unit change in setpoint air temperature results in an average of one-third or more change in the air infiltration rate, and a change of 1.0 °C results in a greater change of air infiltration rate for a larger space. Certainly, the influence of indoor air temperature on air infiltration rate should be attributed to its influence on the indoor-outdoor air temperature difference and thus the buoyancy effect.

3.1.3. Analysis of influencing factors of building airtightness

There are many factors influencing the airtightness of a space. The $\overline{N}$ values of 1#, 3#, and 5# spaces are relatively low (namely, relatively good airtightness). Regarding 1# and 3#, the reason for good airtightness should be the relatively recent renovation, including mainly painting and plastering, which close the tiny gaps and holes in the building envelope. The reason behind 5# should be the large floor area. When all other factors remain the same, a positive correlation of airtightness with the floor area has been observed [30]. The $\overline{N}$ values of 2#, 4#, and 6# spaces are relatively high (namely, relatively poor airtightness). Although all interior doors were closed during the measurements, there were two interior doors in the space 2 # that caused more ALPs. The airtightness of 4# and 6# is the worst because there are interior windows in the space connecting the corridor, where the gaps between the sliders increase the ALPs. As aforementioned, the accurate reasons for the difference in airtightness in these spaces are hard to determine. However, the measurements may indicate that the airtightness of the doors and windows is likely the major contributor.

The measurement results suggest that the effect of seasonal variation on air infiltration is not significant, though it cannot be ignored. According to Tables 7, it can be calculated that the seasonal variation of the air infiltration rate of the six spaces is different. Space 5# is the most affected one, probably due to its orientation towards the south. However, regression calculation indicates that the difference in air infiltration rate of the building in summer and winter is 0.01 h^{-1} with a variation rate of 5.9%, which agrees well with that reported by Mélois et al. [55], namely that the air infiltration of masonry and concrete buildings with insulation layer is negligibly affected by seasonal variations.

By using smoke pens and on-site observations, it is found that there were obvious gaps at the through-wall pipes of split-type air conditioners, which are one of the major factors influencing the building airtightness. This might easily be ameliorated by strengthening the training and education of renovation workers.

3.1.4. Error analysis of the airtightness measurements

During the measurement, it was found that the indoor CO_2 concentration did not peak immediately at the end of the inflation phase, but peaked after a period. Based on several measurements, the buffer time was determined as 5–14 min. Considering that the measurement interval of the instruments is 1.0 min, the relatively long buffer time has a certain influence on the building airtightness

Table 8
The air infiltration rate in summer and winter after the airtightness level of each space is improved (A - initial airtightness level, B - airtightness is improved by one level, C - airtightness is improved by two levels, D - airtightness is improved by three levels, E - airtightness is improved by four levels, F - airtightness is improved by five levels, G - airtightness is improved by six levels, H - airtightness is improved to the highest level).

Season	Space	Air infiltration rate under different working conditions/h^{-1}							
		A	B	C	D	E	F	G	H
Winter	1#	0.13	0.065	0.04	0.02	0.01	0.01	0.01	0.01
	2#	0.21	0.165	0.10	0.065	0.04	0.02	0.01	
	3#	0.15	0.10	0.065	0.04	0.02	0.01	0.01	
	4#	0.36	0.25	0.165	0.10	0.065	0.04	0.02	
	5#	0.13	0.065	0.04	0.02	0.01	0.01	0.01	
	6#	0.34	0.25	0.165	0.10	0.065	0.04	0.02	
Summer	1#	0.14	0.065	0.04	0.02	0.01	0.01	0.01	
	2#	0.26	0.165	0.10	0.065	0.04	0.02	0.01	
	3#	0.15	0.10	0.065	0.04	0.02	0.01	0.01	
	4#	0.33	0.25	0.165	0.10	0.065	0.04	0.02	
	5#	0.21	0.165	0.10	0.065	0.04	0.02	0.01	
	6#	0.39	0.25	0.165	0.10	0.065	0.04	0.02	

measurements using the tracer gas method. This is manifested by the smaller actual decay time and the larger calculated air infiltration rate. It is recommended that the labeling and instruction should be considered in the technical standards for the tracer gas method.

The tracer gas method was time-consuming and laborious, and the fan pressurization method has advantages in this regard, but it could not meet some of the measurement conditions in the present study. In the future, there is still a need to develop suitable testing methods that consider the operation of air-conditioning systems.

3.2. Building simulation

Based on the airtightness classification requirements listed in Table 6 and the $\overline{N}$ values listed in Table 7, the annual cooling and heating loads, as well as the cooling, heating, and fan energy consumption, are calculated based on EnergyPlus simulations. Infiltration models were constructed in the present study to evaluate the influence of airtightness, by considering the air infiltration rate from 0 to 1.0 h^{-1}. Table 8 shows that the reduction of air infiltration rate brought by improving airtightness level by four levels and more is no longer significant.

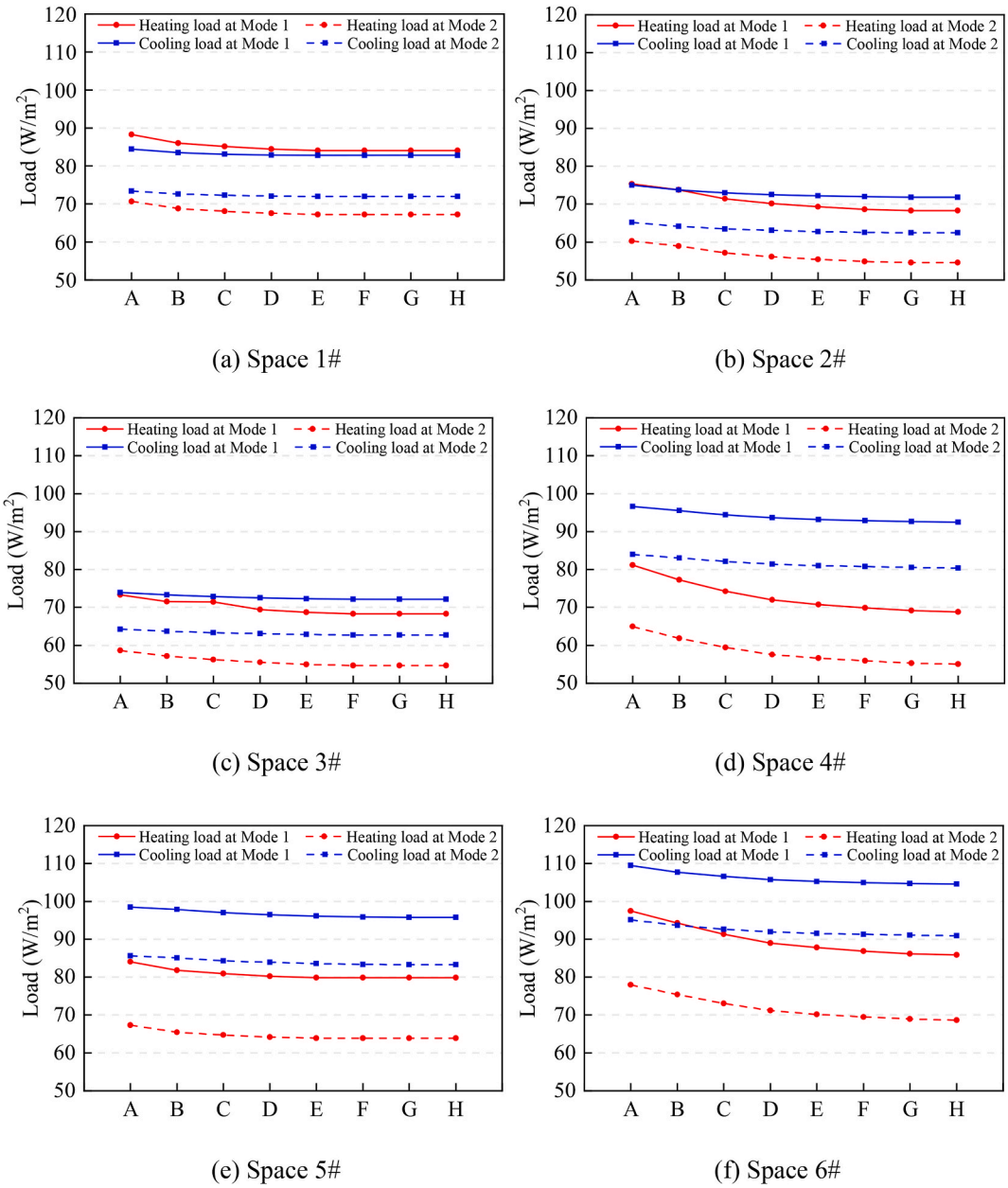

Fig. 9. The changes of cooling and heating loads at the two modes with the improvement of airtightness level.

3.2.1. Infiltration-related energy consumption: effect of air infiltration rate

The values of the cooling and heating loads are simulated to provide reference data for the initial design of the building. Fig. 9 shows the space loads at different airtightness levels in the two ventilation modes. It is found that Mode 1 is more in line with the design requirements than Mode 2 because the space loads at Mode 1 are basically within the index range of 90–120 W/m^2 and 60–90 W/m^2. At the initial airtightness, the loads in all spaces at Mode 2 are approximately 13.0% and 20.0% lower than those at Mode 1. Overall, Mode 1 can reasonably reflect the indoor load.

From Fig. 9, it is found that the heating load of space 1 at Mode 1 is slightly higher than the cooling load, which is different from other spaces, but it is still within acceptable limits. For all spaces, with the improvement of the airtightness level, the average difference in the cooling and heating loads between Mode 1 and Mode 2 varies from 11.7 to 11.3 W/m^2 and from 16.7 to 15.2 W/m^2, respectively. This means that the improvement of the airtightness level weakens the degree of the influence of natural ventilation on the loads.

The improvement of the airtightness level of the building results in a decrease in the load. For all spaces at Mode 1, when the airtightness level is improved by one level, the cooling and heating loads are reduced by 0.6–1.6% and 2.1–4.8%, respectively; when the airtightness level is improved to the highest level 8, the cooling and heating loads are reduced by 2.0–4.4% and 4.8–15.2%, respectively. This indicates that the amplitude of variation in the heating load caused by natural ventilation is more pronounced than that in the cooling load, and the amplitude of variation in the heating load is about three times that of the cooling load.

Subsequently, the simulation of infiltration-related energy consumption is based on Mode 1, and the consideration is that the infiltration-related energy consumption is the difference between the space energy consumption under zero infiltration and actual infiltration conditions. Based on this, simulations are conducted to obtain the infiltration-related energy consumption at different airtightness levels.

As shown in Fig. 10, the total annual infiltration-related energy consumption of the standard floor is 22.84 kWh/m^2·year, accounting for 6.1% of the total annual energy consumption. Among them, the infiltration-related cooling energy consumption is 14.29 kWh/m^2·year, accounting for 10.7% of the total annual cooling energy consumption, and the infiltration-related heating energy consumption is 8.20 kWh/m^2·year, accounting for 21.7% of the total annual heating energy consumption. Due to infiltration, approximately 0.2–3.8% of energy loss is related to cooling and 0.1–2.2% to heating. The proportion of infiltration-related energy consumption for cooling is about twice that of heating, as the energy consumption in the HSCW climate region is contributed mainly by cooling in summer.

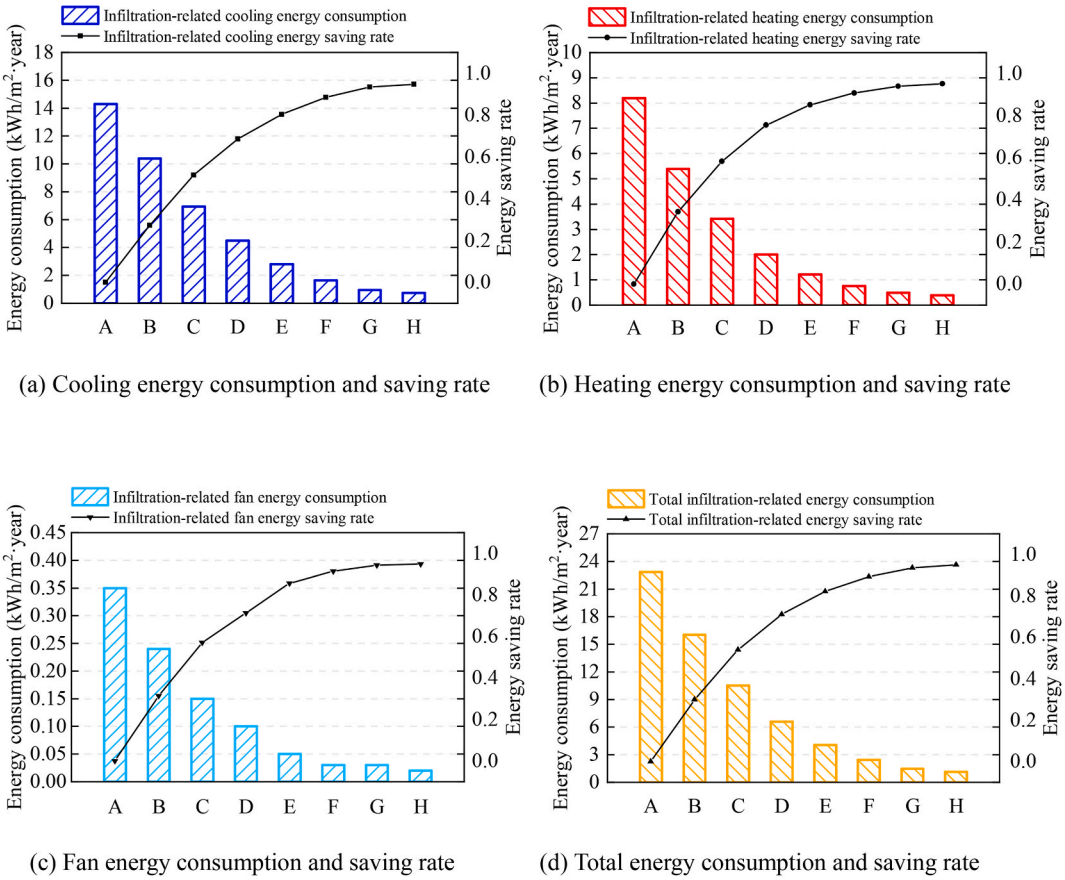

Fig. 10. The infiltration-related energy consumption of the standard floor of the office building at different airtightness levels.

The infiltration-related cooling and heating energy consumption is reduced from 14.29 to 0.75 kWh/m^2·year and from 8.20 to 0.39 kWh/m^2·year, respectively, when the airtightness level is improved from the initial level to the highest level, indicating that the improvement of airtightness level brings considerable energy savings.

Improvement in building airtightness is constrained by building materials, manufacturing technology, and degree of renovation. In addition, considering the limited reduction of loads and energy consumption after improving the airtightness level by four levels and more, it is reasonable to suggest the airtightness of Level 5–6 in the HSCW climate region. Of course, to make the decision, an analysis and detailed assessment of the cost of the measures taken to improve airtightness is required.

3.2.2. Infiltration-related energy consumption: effect of air-conditioning system setpoint air temperature

To evaluate the effect of air-conditioning system setpoint air temperature on the infiltration-related energy consumption, the energy consumption of two spaces was simulated based on the results presented in Fig. 8. The results are presented in Table 9.

As shown in Table 9, the infiltration-related energy consumption increases as the setpoint air temperature drops in summer and rises in winter. The better the space airtightness, the smaller the change in infiltration-related energy consumption caused by the change in air-conditioning setpoint air temperature. When the setpoint air temperature is changed from 28 to 22 °C in summer, the infiltration-related cooling energy consumption is increased by 20.5 and 16.7 kWh/m^2·year for 2# and 3#, respectively, and when the setpoint air temperature is changed from 18 to 24 °C in winter, the infiltration-related heating energy consumption is increased by 12.5 and 8.8 kWh/m^2·year for 2# and 3#, respectively. This means that buildings with poor airtightness have great potential for energy efficiency retrofits, considering the sufficient room for airtightness improvement.

Sixteen different combinations of setpoint air temperatures for summer and winter were considered to further examine the infiltration-related energy consumption, and the results are shown in Fig. 11. The results showed that the distinct combinations of setpoint air temperatures led to different infiltration-related energy consumption. The widely used setpoints, namely Group 10 (26 °C in summer and 20 °C in winter), is not the combination with the lowest infiltration-related energy consumption among the sixteen combinations. This indicates that the infiltration-related energy consumption can be reduced by adjusting the combination of setpoint air temperatures.

As shown in Fig. 11, the infiltration-related energy consumption of the combinations of 28 °C in summer is lower than that of the combinations of 22, 24, and 26 °C in summer. When the setpoint air temperature is changed from 22 to 24 °C, the mean change in infiltration-related cooling and heating energy consumption is 8.2 and 3.9 kWh/m^2·year for the tested spaces. The change in infiltration-related cooling energy consumption is greater than that of infiltration-related heating energy consumption under the same temperature differences. Therefore, adjusting the summer setpoint air temperature is an option that can change the infiltration-related energy consumption to a greater extent. These findings provide information for formulating energy saving measures.

4. Conclusions

Air infiltration is an important factor affecting building energy consumption. At present, the airtightness studies carried out in China focus mainly on the northern region, whereas there is little information available for the southern region. This study performs both on-site measurements and energy simulations to reveal the air infiltration level of buildings in the HSCW climate region and to evaluate its influence on building energy consumption. The main findings are summarized as follows.

(1) The airtightness of the typical building in the HSCW climate region of China is equivalent to Level 3 according to Chinese standard TCECS 704–2020, which reaches the level of most European and American countries. The air infiltration through the masonry and concrete buildings with insulation layer is little affected by seasonal variations (with about 5.9% relative change).
(2) It is necessary to use the air infiltration rate of buildings with the air-conditioning system running to analyze airtightness and its related energy consumption. The operation and setpoint air temperature of an air-conditioning system has a great influence on air infiltration through the building envelope. The mean air infiltration rate with the air-conditioning system running is 1.43–2.24 and 1.34–2.05 times higher than that without air-conditioning system running in summer and winter, respectively. Each unit change in setpoint air temperature can result in an average of one-third or more change in the air infiltration rate.
(3) The air infiltration has an obvious influence on the cooling and heating loads as well as the related energy consumption of buildings in the HSCW climate region. When the air infiltration rate of the office building is reduced from 0.17 h^{-1} to 0.01 h^{-1}, the cooling and heating load is reduced by 2.0–4.4% and 4.8–15.2%, respectively, while the infiltration-related cooling and heating energy consumption is reduced from 14.29 to 0.75 kWh/m^2·year and from 8.20 to 0.39 kWh/m^2·year, respectively. It is reasonable to suggest the airtightness of Level 5–6 for buildings in the HSCW climate region.
(4) The same change in air-conditioning setpoint air temperature in summer and winter results in different changes in infiltration-related energy consumption. When the setpoint air temperature is changed from 22 to 24 °C, the mean change in infiltration-related cooling and heating energy consumption is 8.2 and 3.9 kWh/m^2·year, respectively. It indicates the importance of considering the indoor air temperature when calculating infiltration-related energy consumption.

The airtightness level of buildings in the HSCW climate region and their effects on energy consumption revealed in this study would be useful information and boundary conditions for the performance simulation and assessment of buildings in this region.

Despite the above useful findings, the present study is limited by the small measurement sample, static measurement, and simplified infiltration simulations, which is worthy of further improvement.

Table 9
Total energy consumption at different air-conditioning system setpoint air temperatures in winter and summer.

	Cooling energy consumption/kWh/m^2·year								Heating energy consumption/kWh/m^2·year							
	Zero infiltration 28 °C	Summer case 28 °C	Zero infiltration 26 °C	Summer case 26 °C	Zero infiltration 24 °C	Summer case 24 °C	Zero infiltration 22 °C	Summer case 22 °C	Zero infiltration 18 °C	Winter Case 18 °C	Zero infiltration 20 °C	Winter Case 20 °C	Zero infiltration 22 °C	Winter case 22 °C	Zero infiltration 24 °C	Winter case 24 °C
2#	113.1	124.7	139.4	156.7	167.9	191.7	198.7	230.7	44.4	50.8	61.9	72.0	83.5	98.7	108.6	127.5
3#	114.0	121.3	140.5	151.3	169.3	185.1	200.4	224.4	44.8	49.3	62.5	69.6	84.3	93.6	109.7	123.0

Group 1 - S 22℃ + W 18℃	Group 5 - S 24℃ + W 18℃	Group 9 - S 26℃ + W 18℃	Group 13 - S 28℃ + W 18℃
Group 2 - S 22℃ + W 20℃	Group 6 - S 24℃ + W 20℃	Group 10 - S 26℃ + W 20℃	Group 14 - S 28℃ + W 20℃
Group 3 - S 22℃ + W 22℃	Group 7 - S 24℃ + W 22℃	Group 11 - S 26℃ + W 22℃	Group 15 - S 28℃ + W 22℃
Group 4 - S 22℃ + W 24℃	Group 8 - S 24℃ + W 24℃	Group 12 - S 26℃ + W 24℃	Group 16 - S 28℃ + W 24℃

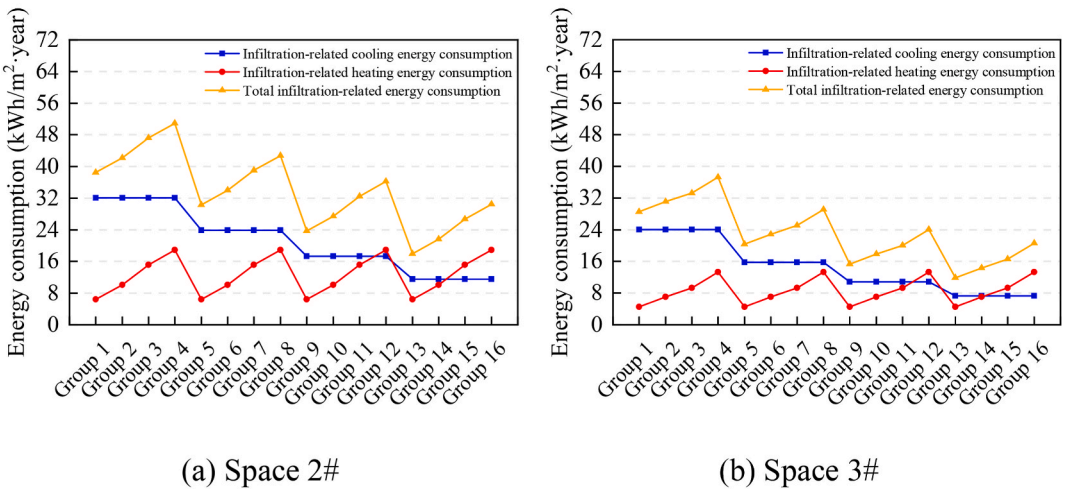

Fig. 11. Infiltration-related energy consumption under different combinations of air-conditioning setpoint air temperatures in summer and winter (S refers to Summer; W refers to Winter).

Author statement

Jie Hu: Writing-original draft, Software, Methodology, Measurement, Formal analysis, Data curation; **Zhengxuan Liu:** Writing-review & editing, Methodology, Supervision; **Guochuan Ma:** Resources, Funding acquisition; **Guoqiang Zhang:** Writing-review & editing, Resources, Funding acquisition; **Zhengtao Ai:** Writing-review & editing, Supervision, Resources, Project administration.

Declaration of competing interest

The authors declare that they have no known competing financial interests or personal relationships that could have appeared to influence the work reported in this paper.

Data availability

Data will be made available on request.

Acknowledgements

This study was supported by the Fundamental Research Funds for the Central Universities (No. 531118010378).

References

[1] C. Younes, C.A. Shdid, G. Bitsuamlak, Air infiltration through building envelopes: a review, J. Build. Phys. 35 (3) (2011) 267–302.
[2] L. Kempton, D. Daly, G. Kokogiannakis, M. Dewsbury, A rapid review of the impact of increasing airtightness on indoor air quality, J. Build. Eng. 57 (2022).
[3] Y. Ji, L. Duanmu, X. Li, Building air leakage analysis for individual apartments in North China, Build. Environ. 122 (2017) 105–115.
[4] J. Langmans, R. Klein, S. Roels, Hygrothermal risks of using exterior air barrier systems for highly insulated light weight walls: a laboratory investigation, Build. Environ. 56 (2012) 192–202.
[5] X. Feng, D. Yan, C. Peng, Analysis of the influence of building airtightness on residential energy consumption, Heating Ventilating and Air Conditioning 44 (2) (2014) 5–14.
[6] J. Feijó-Muñoz, C. Pardal, V. Echarri, J. Fernández-Agüera, R. Assiego de Larriva, M. Montesdeoca Calderín, I. Poza-Casado, M.Á. Padilla-Marcos, A. Meiss, Energy impact of the air infiltration in residential buildings in the Mediterranean area of Spain and the Canary islands, Energy Build. 188–189 (2019) 226–238.
[7] S. Guillén-Lambea, B. Rodríguez-Soria, J.M. Marín, Air infiltrations and energy demand for residential low energy buildings in warm climates, Renew. Sustain. Energy Rev. 116 (2019).
[8] W. Pan, Relationships between air-tightness and its influencing factors of post-2006 new-build dwellings in the UK, Build. Environ. 45 (11) (2010) 2387–2399.
[9] ASHRAE, ANSI/ASHRAE, Standard 62.2: Ventilation and Acceptable Indoor Air Quality in Residential Buildings, 2019.
[10] ISO, ISO 9972-2015 Thermal Performance of Buildings-Determination of Air Permeability of Buildings-Fan Pressurization Method, 2015.
[11] ASTM, ASTME 741-2011(R2017) Standard Test Method for Determining Air Change in a Single Zone by Means of a Tracer Gas Dilution, 2017.
[12] China Academy of Building Research, TCECS 704-2020 Testing and Evaluation Standard for Buildings, Air Tightness, Beijing, 2020.
[13] T. Kalamees, Air tightness and air leakages of new lightweight single-family detached houses in Estonia, Build. Environ. 42 (6) (2007) 2369–2377.
[14] A. Sfakianaki, K. Pavlou, M. Santamouris, I. Livada, M.N. Assimakopoulos, P. Mantas, A. Christakopoulos, Air tightness measurements of residential houses in Athens, Greece, Build. Environ. 43 (4) (2008) 398–405.
[15] D. Sinnott, M. Dyer, Air-tightness field data for dwellings in Ireland, Build. Environ. 51 (2012) 269–275.
[16] W.R. Chan, J. Joh, M.H. Sherman, Analysis of air leakage measurements of US houses, Energy Build. 66 (2013) 616–625.

[17] J. Vinha, E. Manelius, M. Korpi, K. Salminen, J. Kurnitski, M. Kiviste, A. Laukkarinen, Airtightness of residential buildings in Finland, Build. Environ. 93 (2015) 128–140.
[18] F.R.d.A. Alfano, M. Dell'Isola, G. Ficco, F. Tassini, Experimental analysis of air tightness in Mediterranean buildings using the fan pressurization method, Build. Environ. 53 (2012) 16–25.
[19] M. Colijn, A.G. Entrop, M.E. Toxopeus, Evaluating the Effectiveness of Improved Workmanship Quality on the Airtightness of Dutch Detached Houses, 11th Nordic Symposium on Building Physics, 2017. Norway.
[20] A. Salehi, I. Torres, A. Ramos, Experimental analysis of building airtightness in traditional residential Portuguese buildings, Energy Build. 151 (2017) 198–205.
[21] S. Langer, O. Ramalho, M. Derbez, J. Ribéron, S. Kirchner, C. Mandin, Indoor environmental quality in French dwellings and building characteristics, Atmos. Environ. 128 (2016) 82–91.
[22] C.H. Lozinsky, M.F. Touchie, Suite-level air tightness and compartmentalization in multi-unit residential buildings: how do we achieve our intended goals? Build. Environ. 192 (2021).
[23] G. Hong, B.S. Kim, Field measurements of infiltration rate in high rise residential buildings using the constant concentration method, Build. Environ. 97 (2016) 48–54.
[24] S. Shi, C. Chen, B. Zhao, Air infiltration rate distributions of residences in Beijing, Build. Environ. 92 (2015) 528–537.
[25] S. Chen, M.D. Levine, H. Li, P. Yowargana, L. Xie, Measured air tightness performance of residential buildings in North China and its influence on district space heating energy use, Energy Build. 51 (2012) 157–164.
[26] F. Ding, G. Zhang, Y. Yu, J. Lie, Air tightness test of large-scale passive buildings—a case study of the Project of passive house technology experience center in sino-German ecological park, Construction Science and Technology 17 (2016) 34–35+38.
[27] M. Pinto, J. Viegas, V.P. de Freitas, Air permeability measurements of dwellings and building components in Portugal, Build. Environ. 46 (12) (2011) 2480–2489.
[28] X. Liu, T. Zhang, X. Liu, L. Li, L. Lin, Y. Jiang, Energy saving potential for space heating in Chinese airport terminals: the impact of air infiltration, Energy 215 (2021).
[29] H. Zheng, E. Long, Z. Cheng, Z. Yang, Y. Jia, Experimental exploration on airtightness performance of residential buildings in the hot summer and cold winter zone in China, Build. Environ. 214 (2022).
[30] V. Paukštys, G. Cinelis, J. Mockienė, M. Daukšys, Airtightness and heat energy loss of mid-size terraced houses built of different construction materials, Energies 14 (19) (2021).
[31] J. Feijó-Muñoz, R.A. González-Lezcano, I. Poza-Casado, M.Á. Padilla-Marcos, A. Meiss, Airtightness of residential buildings in the Continental area of Spain, Build. Environ. 148 (2019) 299–308.
[32] H. Tommerup, J. Rose, S. Svendsen, Energy-efficient houses built according to the energy performance requirements introduced in Denmark in 2006, Energy Build. 39 (10) (2007) 1123–1130.
[33] Z. Wang, Z. Li, J. Shi, L. Di, L. Wei, Review and Analysis on Foreign and Domestic Standards on Building External Envelope Overall Air Tightness, 3rd International Conference on Education, Management, Arts, Economics and Social Science, 2015.
[34] M. Wang, K. Qin, E. Long, W. Liang, P. Ding, The influence of building envelope tightness on office building energy, Refrig. Air Cond. 30 (3) (2016) 345–349.
[35] J. Jokisalo, J. Kurnitski, M. Korpi, T. Kalamees, J. Vinha, Building leakage, infiltration, and energy performance analyses for Finnish detached houses, Build. Environ. 44 (2) (2009) 377–387.
[36] J. Šadauskienė, L. Šeduikytė, V. Paukštys, K. Banionis, A. Gailius, The role of air tightness in assessment of building energy performance: case study of Lithuania, Energy for Sustainable Development 32 (2016) 31–39.
[37] Background Analysis of Changsha Climate, China Weather Network, http://www.weather.com.cn/cityintro/101250101.shtml.
[38] J. Hou, Y. Sun, Q. Chen, R. Cheng, J. Liu, X. Shen, H. Tan, H. Yin, K. Huang, Y. Gao, X. Dai, L. Zhang, B. Liu, J. Sundell, Air change rates in urban Chinese bedrooms, Indoor Air 29 (5) (2019) 828–839.
[39] V.E.M. Cardoso, P.F. Pereira, N.M.M. Ramos, R.M.S.F. Almeida, The impacts of air leakage paths and airtightness levels on air change rates, Buildings 10 (3) (2020).
[40] W. Liu, X. Zhao, Q. Chen, A novel method for measuring air infiltration rate in buildings, Energy Build. 168 (2018) 309–318.
[41] D.-S. Lee, J.-W. Jeong, J.-H. Jo, Experimental study on airtightness test methods in large buildings; proposal of averaging pressure difference method, Build. Environ. 122 (2017) 61–71.
[42] S. Cui, M. Cohen, P. Stabat, D. Marchio, CO_2 tracer gas concentration decay method for measuring air change rate, Build. Environ. 84 (2015) 162–169.
[43] S. Hormigos-Jimenez, M.A. Padilla-Marcos, A. Meiss, R.A. Gonzalez-Lezcano, J. Feijó-MuÑoz, Experimental validation of the age-of-the-air CFD analysis: a case study, Science and Technology for the Built Environment 24 (9) (2018) 994–1003.
[44] Y.-S. Hsu, X. Zheng, D. Kraniotis, M. Gillott, S.-K. Lee, C.J. Wood, The impact of wind upon the Pulse technique measured airtightness of a detached dwelling, Build. Environ. 215 (2022).
[45] S.M. H, Estimation of infiltration from leakage and climate indicators, Energy Build. 10 (1) (1987) 81–86.
[46] Beijing Building Research Institute Corporation Limited of CSCEC, DB11/T 555-2015 Standard for On-Site Testing of Energy Efficient Civil Buildings Engineering, 2015. Beijing.
[47] R. Gil-Valverde, D. Tamayo-Alonso, A. Royuela-del-Val, I. Poza-Casado, A. Meiss, M.Á. Padilla-Marcos, Three-dimensional characterization of air infiltration using infrared thermography, Energy Build. 233 (2021).
[48] L. Tang, Z. Ai, C. Song, G. Zhang, Z. Liu, A strategy to maximally utilize outdoor air for indoor thermal environment, Energies 14 (13) (2021).
[49] L.C. Ng, W.S. Dols, S.J. Emmerich, Evaluating potential benefits of air barriers in commercial buildings using NIST infiltration correlations in EnergyPlus, Build. Environ. 196 (2021).
[50] Z. Sardoueinasab, P. Yin, D. O'Neal, Energy modeling and analysis of inherent air leakage from parallel fan-powered terminal units using EMS in EnergyPlus, Energy Build. 176 (2018) 109–119.
[51] Y. Liu, B. Li, R. Yao, X. Cao, Influence of building airtightness on energy consumption of office building in chongqing, in: Proceedings of the 11th International Symposium on Heating, Ventilation and Air Conditioning (ISHVAC 2019), 2020, pp. 137–145.
[52] Y. Hu, Z. Liu, Z. Ai, G. Zhang, Performance evaluation of ventilative cooling systems for buildings under different control parameters and strategies, J. Build. Eng. 65 (2023).
[53] H. Li, T. Hong, M. Sofos, An inverse approach to solving zone air infiltration rate and people count using indoor environmental sensor data, Energy Build. 198 (2019) 228–242.
[54] Ministry of Housing and Urban-Rural Development of the People's Republic of China, GB 55015-2021 General Code for Energy Efficiency and Renewable Energy Application in Buildings, 2021. Beijing.
[55] A.B. Mélois, B. Moujalled, G. Guyot, V. Leprince, Improving building envelope knowledge from analysis of 219,000 certified on-site air leakage measurements in France, Build. Environ. 159 (2019).